

Article

Uptake of Be(II) by Cement in Degradation Stage I: Wet-Chemistry and Molecular Dynamics Studies

Neşe Çevirim-Papaioannou ^{1,*}, Sangsoo Han ², Iuliia Androniuk ¹, Wooyong Um ², Marcus Altmaier ¹ 
and Xavier Gaona ^{1,*} 

¹ Institute for Nuclear Waste Disposal (INE), Karlsruhe Institute of Technology (KIT), 76021 Karlsruhe, Germany; iuliia.androniuk@kit.edu (I.A.); marcus.altmaier@kit.edu (M.A.)

² Division of Advanced Nuclear Engineering (DANE), Pohang University of Science and Technology (POSTECH), 77 Chongam-ro, Pohang 790-784, Korea; sshan1214@postech.ac.kr (S.H.); wooyongum@postech.ac.kr (W.U.)

* Correspondence: nese.cevirim@kit.edu (N.Ç.-P.); xavier.gaona@kit.edu (X.G.)

Abstract: The uptake of beryllium by hardened cement paste (HCP, with CEM I 42,5 N BV/SR/LA type) in degradation stage I was investigated with a series of batch sorption experiments with $10^{-6} \text{ M} \leq [\text{Be(II)}]_0 \leq 10^{-2.5} \text{ M}$ and $2 \text{ g}\cdot\text{L}^{-1} \leq [\text{S/L}] \leq 50 \text{ g}\cdot\text{L}^{-1}$. All experiments were performed under Ar atmosphere at $T = (22 \pm 2) \text{ }^\circ\text{C}$. Solubility limits calculated for $\alpha\text{-Be(OH)}_2(\text{cr})$ in the conditions of the cement pore water were used to define the experimental window in the sorption experiments. Beryllium sorbs strongly on HCP under all of the investigated conditions, with $\log R_d \approx 5.5$ (R_d in $\text{L}\cdot\text{kg}^{-1}$). Sorption isotherms show a linear behavior with a slope of $\approx +1$ ($\log [\text{Be(II)}]_{\text{solid}}$ vs. $\log [\text{Be(II)}]_{\text{aq}}$) over four orders of magnitude ($10^{-8} \text{ M} \leq [\text{Be(II)}]_{\text{aq}} \leq 10^{-4} \text{ M}$), which confirm that the uptake is controlled by sorption processes and that solubility phenomena do not play any role within the considered boundary conditions. The similar uptake observed for beryllium in calcium silicate hydrate (C-S-H) phases supports that the C-S-H phases are the main sink of Be(II) in cement. The strong uptake observed for Be(II) agrees with the findings reported for heavier metal ions, e.g., Zn(II), Eu(III), Am(III), or Th(IV). The exceptional sorption properties of beryllium can be partially explained by its small size, which result in a charge-to-size ratio (z/d) of the same order as Eu(III) or Am(III). Kinetic experiments confirm the slow uptake of Be(II), which is characterized by a two-step process. In analogy to other strongly sorbing metal ions such as Zn(II) or Th(IV), a fast surface complexation ($t < 4$ days) followed by a slower incorporation of Be(II) in the C-S-H structure ($t \geq 60$ days) are proposed. The surface complexation was studied in detail with molecular dynamic simulations, and the most common surface species are identified and described. This work provides the first experimental evidence supporting the strong uptake of Be(II) by HCP in degradation stage I, further extending previous findings on C-S-H phases and HCP in degradation stage II. These results overcome previous conservative estimates assuming no or only a weak uptake in cementitious systems and represent a relevant contribution for the quantitative assessment on the retention/mobilization of beryllium in the context of nuclear waste disposal.

Keywords: beryllium; cement; sorption; degradation stage I; molecular dynamics



Citation: Çevirim-Papaioannou, N.; Han, S.; Androniuk, I.; Um, W.; Altmaier, M.; Gaona, X. Uptake of Be(II) by Cement in Degradation Stage I: Wet-Chemistry and Molecular Dynamics Studies. *Minerals* **2021**, *11*, 1149. <https://doi.org/10.3390/min11101149>

Academic Editor:
Andrey G. Kalinichev

Received: 3 September 2021
Accepted: 12 October 2021
Published: 18 October 2021

Publisher's Note: MDPI stays neutral with regard to jurisdictional claims in published maps and institutional affiliations.



Copyright: © 2021 by the authors. Licensee MDPI, Basel, Switzerland. This article is an open access article distributed under the terms and conditions of the Creative Commons Attribution (CC BY) license (<https://creativecommons.org/licenses/by/4.0/>).

1. Introduction

Beryllium is a relatively rare element found in the Earth's crust in a concentration of 4–6 ppm [1]. It is a component in more than 50 minerals, with the two main ores being beryl ($\text{Al}_2\text{Be}_3\text{Si}_6\text{O}_{18}$) and bertrandite ($\text{Be}_4\text{Si}_2\text{O}_7(\text{OH})_2$) [1]. In the nuclear field, beryllium is used in the moderators and reflectors for research reactors due to its low thermal neutron absorption cross-section and specific chemical/structural properties [2–4]. Due to the alteration of its mechanical properties, irradiated components containing beryllium need to be replaced and disposed of in underground repositories for nuclear waste.

In aqueous systems, beryllium is only expected in the +II oxidation state. The solubility and hydrolysis of Be(II) have been extensively studied under acidic conditions [5–10], but the number of experimental studies is very limited in the alkaline to hyperalkaline conditions [5,11–13]. The recent work by Çevirim-Papaioannou and co-workers represents the most systematic solubility study of Be(II) with a focus on the alkaline pH conditions of relevance for cementitious systems [13]. In combination with extensive solid phase characterization and ^9Be NMR, the authors provided comprehensive chemical, thermodynamic, and activity models for the system $\text{Be}^{2+}\text{-Na}^+\text{-K}^+\text{-H}^+\text{-Cl}^-\text{-OH}^-\text{-H}_2\text{O(l)}$. These models allow the calculation of the solubility of Be(II) over a broad pH-range, whilst predicting the predominance of the hydrolysis species $\text{Be(OH)}_2\text{(aq)}$, Be(OH)_3^- and Be(OH)_4^{2-} within $10 \leq \text{pH} \leq 13.3$, i.e., covering the complete range of pH defined by the different degradation stages of cement.

Cement is one of the materials considered for the stabilization of the waste and for construction purposes, and hence it is part of the multi-barrier system in some of the repository concepts for nuclear waste. In contact with groundwater, cementitious materials undergo a degradation process following three main degradation stages [14–18]. The first degradation stage is controlled by the dissolution of Na and K oxo/hydroxides, which result in high pH values (≈ 13.3) and high concentrations of both alkalis, i.e., $[\text{Na}] \approx 0.11 \text{ M}$ and $[\text{K}] \approx 0.18 \text{ M}$. After the full dissolution of Na and K oxo/hydroxides, the pore water composition in degradation stage II is mostly controlled by the dissolution of portlandite (Ca(OH)_2), which buffers the pH at ≈ 12.5 whilst retaining high concentrations of Ca in the pore water, i.e., $[\text{Ca}] \approx 0.02 \text{ M}$. Calcium silicate hydrates (C-S-H) with Ca : Si ratios of 1.5 to 0.6, which are the last cement phases to be dissolved/degraded, and buffer the pH in degradation stage III of cement formation, and ≈ 12.5 to ≈ 10 . C-S-H phases are considered to be among the most important cement components governing the uptake of metal ions [16,19]. The retention mechanisms include not only surface complexation, but also incorporation in the CaO-layer as well as in the interlayer of the C-S-H structure [17].

With the exception of the recent work by Çevirim-Papaioannou and co-workers dedicated to the uptake of Be(II) by C-S-H phases and HCP in degradation stage II (Çevirim-Papaioannou et al. 2021), no experimental studies investigating the uptake of Be(II) by cementitious materials are available in the literature. Although acknowledging that an average to strong uptake might be expected on the basis of the high charge-to-size ratio (z/d) of the Be^{2+} ion, most of the reference works (sorption databases, safety assessments of waste management organizations, reference books) assume no or weak sorption of beryllium by cement [16,18–23]. In the “Cementitious Near-Field Sorption Data Base for Performance Assessment of an ILW Repository in Opalinus Clay”, Wieland and Van Loon (2003) acknowledged that the uptake of beryllium by hardened cement paste (HCP) is likely, but set the sorption value to zero and also considered the possible competition imposed by the strong hydrolysis of Be(II) and the predominance of the anionic species Be(OH)_3^- and Be(OH)_4^{2-} [13]. The same criteria was retained in the updated sorption database reported by Wieland in 2014 [19]. In the Dossier 2005 Argile (Tome: Évaluation de Sûreté du Stockage Géologique), Andra assumed a retardation coefficient for ^{10}Be in concrete of 1, which implies no sorption [20]. A small inventory of beryllium arising from the decommissioning of a research reactor in Studsvik (estimated as 300 kg, with $2.7 \times 10^{10} \text{ Bq}$ in ^{10}Be) is expected to be disposed of in SFL, the planned Swedish repository for long-lived low- and intermediate-level radioactive waste [21–23]. In the compilation of data for the analysis of radionuclide migration from SFL, Skagius and co-workers proposed a distribution coefficient of $0.05 \text{ m}^3 \cdot \text{kg}^{-1}$ for the uptake of beryllium by concrete [24,25]. This value was based on the direct analogy with radium, which can be put on doubt by considering the large difference in the ionic radii of both metal ions ($r_{\text{Be}^{2+}} = 0.27 \text{ \AA}$ and $r_{\text{Ra}^{2+}} = 1.48 \text{ \AA}$, with coordination numbers $\text{CN} = 4$ and 8, respectively) [26]. In their report dedicated to the toxicity screening assessment for the Nirex phased geological disposal concept, Hunter and co-workers acknowledged the lack of experimental data for the uptake

of beryllium in cement and proposed a distribution coefficient of $1 \times 10^{-4} \text{ m}^3 \cdot \text{kg}^{-1}$ based on near-field data [27,28].

The discussion above evidences the need of experimental data for the uptake of beryllium by cementitious materials. In the context of the EU-funded collaborative project “Cement-based materials, properties, evolution, barrier functions” (Cebama), this study aims at a quantitative description of the beryllium uptake by cement HCP in degradation stage I under a range of initial beryllium concentrations ($[\text{Be}]_0$) and solid-to-liquid ratios (S/L). The present work complements and further expands the experimental study by Çevirim-Papaioannou et al., which was dedicated to the uptake of beryllium by HCP in degradation stage II and C-S-H phases [13].

2. Experimental

2.1. Chemicals

Samples were prepared, handled, and equilibrated at $T = (22 \pm 2) \text{ }^\circ\text{C}$ in an Ar-glove box with $\text{O}_2 < 1 \text{ ppm}$. All solutions were prepared using purified water (Milli-Q academic, Millipore, $18.2 \text{ M}\Omega \cdot \text{cm}$) purged with Ar for $\approx 1 \text{ h}$ to remove dissolved $\text{CO}_2(\text{g})$. $\text{BeSO}_4 \cdot 4\text{H}_2\text{O}$ (99.99%), NaOH Titrisol, KOH Titrisol, and HCl Titrisol were obtained from Merck. $\text{Na}_2\text{O}_7\text{Si}_3$ and $\text{Ca}(\text{OH})_2$ were of analytical grade and were purchased from Merck.

2.2. Cement and Cement Pore Water

A hydrated cement paste (HCP) with CEM I 42.5 N BV/SR/LA type was provided by the Swedish Nuclear Fuel and Waste Management Company (SKB) (see [29] for more details). The first 2.5 mm of the cement monolith were cut off to remove the possibly carbonated surface. The remaining HCP material was milled, sieved to a particle size of $< 100 \text{ }\mu\text{m}$, and stored under Ar atmosphere. The HCP powder was extensively characterized at KIT-INE in a previous study by Tasi and co-workers using X-ray diffraction (XRD), thermogravimetry/differential thermal analysis (TG-DTA), X-ray photoelectron spectroscopy (XPS), and Brunauer-Emmett-Teller (BET) surface area [29].

Artificial cement porewater (ACW) corresponding to degradation stage I was prepared based on the pore water composition reported by Lagerblad and Trägårdhof for the same cement formulation [30,31], i.e., $[\text{Na}] = 0.028 \text{ M}$, $[\text{K}] = 0.083 \text{ M}$, $[\text{Ca}] = 9 \times 10^{-4} \text{ M}$, $[\text{Si}] = 8 \times 10^{-4} \text{ M}$ and a pH of 13.06. Aluminum and sulfate were disregarded in the preparation of the ACW due to the low concentration of both components in the reported pore water, $[\text{Al}] = [\text{SO}_4] = 4 \times 10^{-5} \text{ M}$.

2.3. Sorption Experiments

Sorption samples were prepared with 20 mL of ACW and the corresponding amount of HCP to attain $2 \text{ g} \cdot \text{L}^{-1} \leq [\text{S}/\text{L}] \leq 50 \text{ g} \cdot \text{L}^{-1}$. Stock solutions with $[\text{BeSO}_4]_{\text{aq}} = 0.35\text{--}10^{-3} \text{ M}$ were used to obtain the targeted initial Be concentrations of $1 \times 10^{-6} \text{ M} \leq [\text{Be}]_0 \leq 0.03 \text{ M}$. Experimental solubility data and thermodynamic models reported in Çevirim-Papaioannou et al. (2020) [13] for $\alpha\text{-Be}(\text{OH})_2(\text{cr})$ in NaCl-NaOH and KCl-KOH systems were considered for the definition of the initial beryllium concentrations in the sorption experiments (see also Section 3). Sorption kinetics were monitored for $t \leq 145 \text{ days}$.

Total concentrations of Be(II) and major ions (Ca, Na, K, and Si) in the aqueous phase were quantified by inductively coupled plasma mass spectroscopy (ICP-MS, Perkin Elmer ELAN 6100) and inductively coupled plasma optical emission spectroscopy (ICP-OES, Perkin-Elmer 4300 DV) after ultrafiltration with 10 kD filters (2–3 nm cut-off Nanosep[®] centrifuge tubes, Pall Life Sciences). The detection limit of ICP-MS for the quantification of beryllium in the conditions of our experiments ($\approx 10^{-8} \text{ M}$) was calculated as 3 times the standard deviation of the blank.

Distribution ratios, R_d (in $L \cdot kg^{-1}$), were calculated as the ratio of beryllium concentration in the solid phase ($[Be]_{solid}$, in $mol \cdot kg^{-1}$) and aqueous solution ($[Be]_{aq}$, in M):

$$R_d = \frac{[Be]_{solid}}{[Be]_{aq}} \cdot \frac{V}{m} = \frac{[Be]_0 - [Be]_{aq}}{[Be]_{aq}} \cdot \frac{V}{m} \quad (1)$$

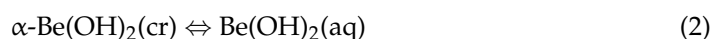
where $[Be]_0$ is the initial beryllium concentration in the aqueous phase, V is the volume of sample (L), and m is the mass of HCP (kg). Sorption isotherms were represented as $\log [Be]_{solid}$ vs. $\log [Be]_{aq}$.

2.4. Computational Methods

Classical molecular dynamics (MD) was used to study surface complexes of beryllium on the (001) C-S-H surface [32]. The structure of C-S-H with Ca:Si = 0.5 reported by Jamil et al. [32] was modified as follows: all the bridging Si on the surface were removed, the silanol groups were deprotonated, and the missing Si were replaced by Ca^{2+} . This results in a C-S-H with Ca:Si > 1.4, as expected in the cement paste investigated in this work. The interfacial aqueous solution contained six ions of $Be(OH)_3^-$, and four ions of $Be(OH)_4^{2-}$ with ~5400 H_2O molecules, which corresponds approximately to a 0.1 M beryllium ion concentration and a pH of ~12.7, as estimated using reported thermodynamic data [33]. The formation of polynuclear species at this high Be(II) concentration was evaluated by molecular dynamics and disregarded in [33]. The interatomic interaction parameters for C-S-H and H_2O were taken from the ClayFF [34] and its later modifications for cement systems [35,36]. The 12-6-4 LennardJones type non-bonded parameters for Ca^{2+} and Be^{2+} , which include the contribution from the ion-induced dipole interaction, were taken from Li and Merz [30]. The main MD production run was performed for 5 ns (NVT-ensemble, $T = 300$ K, timestep = 1 fs). All simulations were performed using the LAMMPS software package (3 March 2020 version) [37].

3. Solubility and Aqueous Speciation of Be(II) in ACW

Chemical, thermodynamic, and activity models reported in Çevirim-Papaioannou et al. for the solubility and hydrolysis of Be(II) in NaCl-NaOH and KCl-KOH solutions were considered to calculate the solubility upper limits and the precise aqueous speciation of Be(II) in ACW [13]. The three main equilibrium reactions controlling the solubility and hydrolysis of beryllium in cementitious systems with $10 \leq pH \leq 13.3$ are defined as:



with

$$\log {}^*K'_{s,(1,2)} = \log {}^*K^\circ_{s,(1,2)} = \log [\text{Be(OH)}_2(\text{aq})] \quad (5)$$

$$\log {}^*K'_{s,(1,3)} = \log [\text{Be(OH)}_3^-] + \log [\text{H}^+] = \log {}^*K^\circ_{s,(1,3)} - \log \gamma_{\text{Be(OH)}_3^-} - \log \gamma_{\text{H}^+} + \log a_w \quad (6)$$

$$\log {}^*K'_{s,(1,4)} = \log [\text{Be(OH)}_4^{2-}] + 2 \log [\text{H}^+] = \log {}^*K^\circ_{s,(1,4)} - \log \gamma_{\text{Be(OH)}_4^{2-}} - 2 \log \gamma_{\text{H}^+} + 2 \log a_w \quad (7)$$

where $\log {}^*K^\circ_{s,(1,x)}$ and $\log {}^*K'_{s,(1,x)}$ are the solubility constants at the reference state ($I = 0$) and the conditional solubility constants at a given ionic strength ($I > 0$), respectively, γ is the activity coefficient of a given ion, and a_w is the activity of water at a given background electrolyte concentration. The specific ion interaction (SIT) theory and the SIT coefficients reported in Çevirim-Papaioannou et al. (2020) [13] for $\epsilon(\text{Be(OH)}_x^{2-x}, \text{Na}^+)$ and $\epsilon(\text{Be(OH)}_x^{2-x}, \text{K}^+)$ are considered to extrapolate the values of $\log {}^*K^\circ_{s,(1,x)}$ to the pore water composition in ACW and thus to calculate the solubility and fraction diagrams shown in Figure 1.

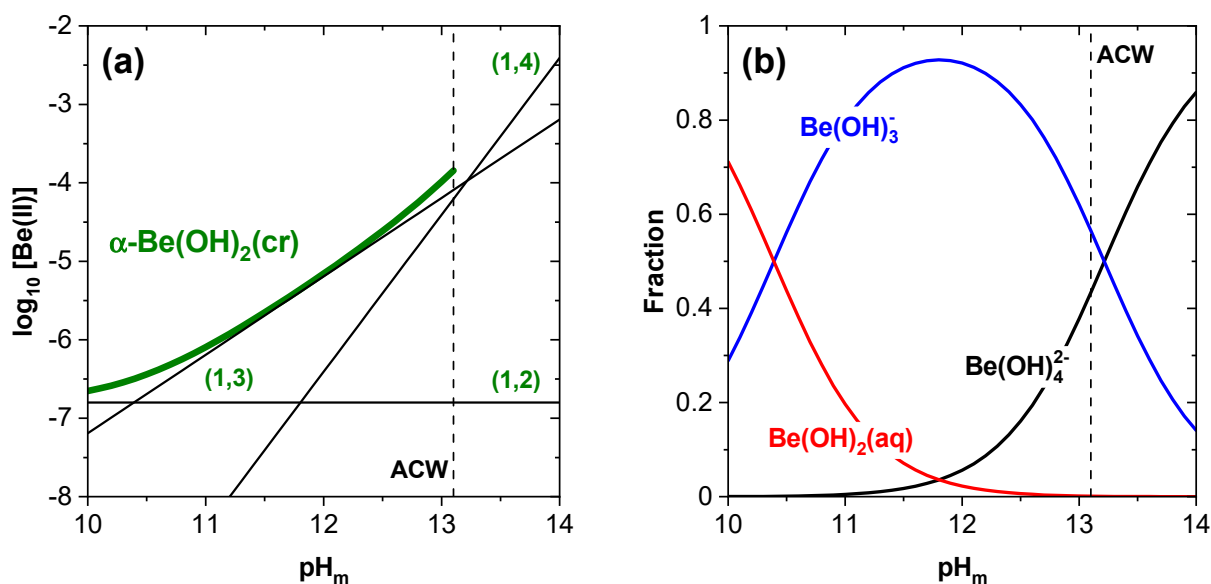


Figure 1. (a) Solubility and (b) fraction diagrams of Be(II) within $10 \leq \text{pH}_m \leq 14$ calculated for the pore water composition of ACW using the chemical, thermodynamic, and activity models reported in [13].

The solubility calculations in Figure 1a show a clear increase in the concentration of beryllium with increasing pH_m due to the formation of anionic hydrolysis species in equilibrium with $\alpha\text{-Be(OH)}_2(\text{cr})$. The solubility limit calculated at $\text{pH}_m = 13.1$ is $[\text{Be(II)}] \approx 10^{-4}$ M, which represents an upper concentration limit for beryllium in ACW. This upper limit was considered as key input in the definition of the experimental window of the sorption experiments. The aqueous speciation of Be(II) in ACW is dominated by close to equimolar concentrations of Be(OH)_3^- and Be(OH)_4^{2-} , i.e., negatively charged species are responsible for the interaction of Be(II) with cement in degradation stage I. Note that the predominance of anionic hydrolysis species was raised in previous studies as a possible argument to predict a weak or no uptake of beryllium by cement [16,18].

4. Results and Discussion

4.1. Pore Water Composition

Table 1 summarizes the pore water composition (pH , $[\text{Na}]$, $[\text{K}]$, $[\text{Ca}]$, $[\text{Si}]$) in ACW equilibrated with HCP in the absence and presence of beryllium (1×10^{-6} M $\leq [\text{Be}]_0 \leq 0.03$ M) at $\text{S/L} = 2\text{--}50$ g·L $^{-1}$. Table 1 also shows the composition of ACW in the original recipe before equilibration with cement and beryllium.

Nearly constant values of pH , $[\text{Na}]$, $[\text{K}]$, and $[\text{Ca}]$ are measured after the equilibration of ACW with cement and beryllium with $[\text{Be}]_0$ below $\approx 10^{-3}$ M, which support that the cement material was not altered over the course of the sorption experiments. The increase in the Ca concentration observed after equilibrating ACW with cement can be attributed to the slight undersaturation conditions of the original recipe with respect to $\text{Ca(OH)}_2(\text{s})$, as calculated using the ThermoChimie database ($[\text{Ca}] \approx 3 \times 10^{-3}$ M at $\text{pH} = 13.06$) [38].

Table 1 shows that the pore water composition (in terms of pH and $[\text{Ca}]$) is impacted at $[\text{Be}]_0 \geq 1 \times 10^{-3}$ M. The observed decrease in pH is rationalized by the consumption of the OH^- that is required for the formation of Be(OH)_3^- and Be(OH)_4^{2-} from the initial Be^{2+} spiked to ACW. For this reason, the samples highlighted in *cursive* in Table 1 are not considered in the discussion of sorption isotherms in Section 4.3.

Table 1. Aqueous composition (pH, [Na], [K], [Ca], [Si]) of the pore water in contact with HCP (deg. stage I) before and after equilibration with beryllium. Related uncertainties are ± 0.10 for pH measurements and $\pm 2\text{--}30\%$ for the measured concentrations.

	[Be] ₀ [M]	pH	Na [M]	K [M]	Ca [M]	[Si] [M]
ACW recipe		13.06	0.028	0.083	9.0×10^{-4}	8×10^{-4}
ACW contacted with HCP Absence of Be(II); S/L = 2 g·L ⁻¹		13.10	0.032	0.076	3.7×10^{-3}	
ACW contacted with HCP Presence of Be(II); S/L = 2 g·L ⁻¹	1×10^{-6} M	13.10	0.034	0.076	3.8×10^{-3}	
	3×10^{-6} M	13.04	0.032	0.080	4.0×10^{-3}	
	1×10^{-5} M	13.09	0.031	0.075	3.4×10^{-3}	
	3×10^{-5} M	13.14	0.029	0.078	3.4×10^{-3}	
	1×10^{-4} M	13.04	0.033	0.079	3.8×10^{-3}	
	3×10^{-4} M	13.03	0.032	0.081	3.7×10^{-3}	
	1×10^{-3} M	13.02	0.032	0.077	3.5×10^{-3}	
	3×10^{-3} M	12.98	0.032	0.079	2.0×10^{-3}	
	0.03 M	12.85	0.032	0.070	1.5×10^{-3}	
ACW contacted with HCP Presence of Be(II); S/L = 10 g·L ⁻¹	1×10^{-6} M	13.05	0.031	0.082	4.0×10^{-3}	
	3×10^{-6} M	13.09	0.036	0.088	4.2×10^{-3}	
	1×10^{-5} M	13.07	0.029	0.076	3.7×10^{-3}	
	3×10^{-5} M	13.06	0.031	0.082	4.0×10^{-3}	
	1×10^{-4} M	13.08	0.032	0.084	4.0×10^{-3}	
	3×10^{-4} M	13.05	0.032	0.084	3.9×10^{-3}	
	1×10^{-3} M	13.02	0.033	0.081	4.0×10^{-3}	
	0.03 M	13.01	0.032	0.082	4.3×10^{-3}	
ACW contacted with HCP Presence of Be(II); S/L = 20 g·L ⁻¹	3×10^{-5} M	13.07	0.032	0.079	4.1×10^{-3}	
	1×10^{-4} M	13.08	0.035	0.087	4.6×10^{-3}	
	3×10^{-4} M	13.09	0.034	0.083	4.3×10^{-3}	
	1×10^{-3} M	13.10	0.035	0.078	4.3×10^{-3}	
	3×10^{-3} M	12.97	0.028	0.075	5.6×10^{-3}	
	0.03 M	12.96	0.032	0.083	4.1×10^{-3}	
ACW contacted with HCP Presence of Be(II); S/L = 50 g·L ⁻¹	3×10^{-5} M	13.07	0.034	0.086	4.6×10^{-3}	
	1×10^{-4} M	13.10	0.032	0.088	4.7×10^{-3}	
	3×10^{-4} M	13.06	0.030	0.084	4.4×10^{-3}	
	1×10^{-3} M	13.05	0.030	0.084	4.4×10^{-3}	
	3×10^{-3} M	13.05	0.027	0.084	4.0×10^{-3}	
	0.03 M	12.96	0.029	0.078	5.1×10^{-3}	

4.2. Sorption Kinetics

The uptake of Be(II) by HCP in degradation stage I (expressed in terms of $\log R_d$ values, with R_d in $\text{L}\cdot\text{kg}^{-1}$) shows slow sorption kinetics (Figure 2). A first, the fast uptake of Be(II) ($\log R_d \approx 4.5$ after 4 days) is followed by a slower increase in the distribution coefficients, which reach steady state conditions after only ≈ 60 days. Figure 2 also shows the evolution of the beryllium concentration as a function of time (right Y-axis in Figure 2). The initial beryllium concentration ($[\text{Be}]_0 = 3 \times 10^{-3}$ M) drops ($t < 4$ days) below the

solubility limit of $\alpha\text{-Be(OH)}_2(\text{cr})$ in ACW ($\approx 10^{-4}$ M see Section 3) very quickly. This indicates that solubility phenomena have no or a very minor impact on the experimental observations collected within the kinetic study.

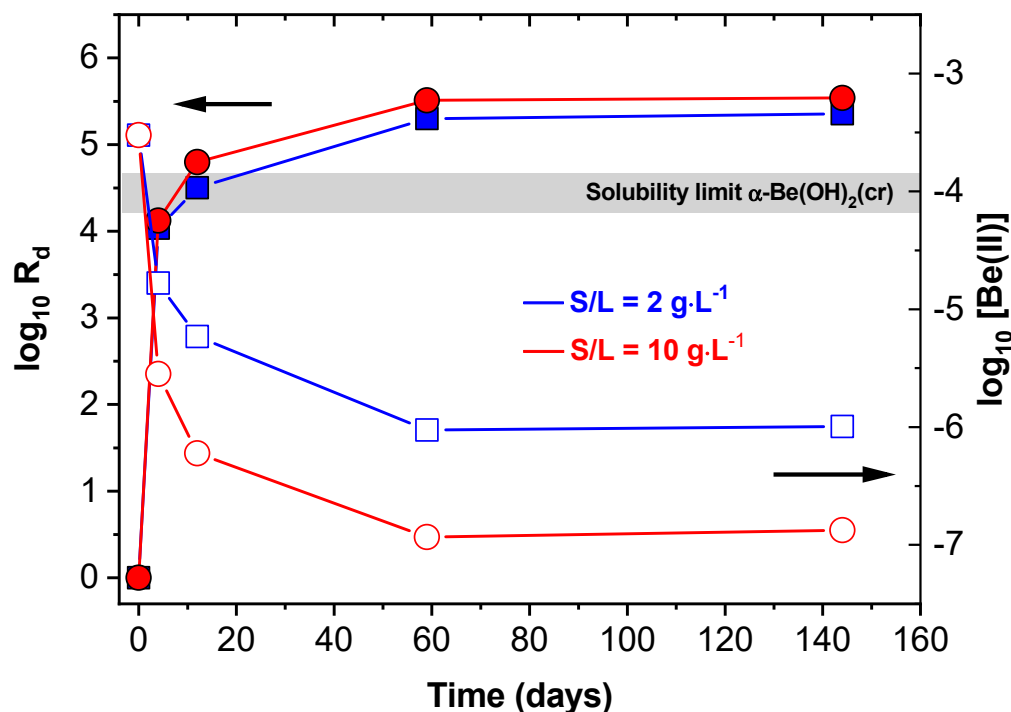


Figure 2. Kinetics of the Be(II) uptake by HCP in degradation stage I with $[\text{Be}]_0 = 3 \times 10^{-4}$ and $S/L = 2$ and $10 \text{ g}\cdot\text{L}^{-1}$. Sorption kinetics expressed in terms of $\log R_d$ values (left Y-axis, with R_d expressed in $\text{L}\cdot\text{kg}^{-1}$) and Be(II) concentrations (right Y-axis) as a function of time. Grey region defines the solubility limit of $\alpha\text{-Be(OH)}_2(\text{cr})$ in ACW.

In their sorption study with HCP in degradation stage II and with C-S-H phases, Çevirim-Papaioannou et al. reported very similar, two-step kinetic behaviour for the uptake of Be(II) [33]. The $\log R_d$ values reported by these authors for C-S-H phases with Ca:Si = 1.6 are of the same order as the distribution coefficients determined in this work for HCP in degradation stage I, thus supporting that C-S-H phases are the main sink of Be(II) in cement.

As described for other strongly sorbing metal ions, the two-step uptake observed for beryllium can be interpreted with a first, fast surface complexation process followed by the incorporation of beryllium in the structure of C-S-H, most likely in the interlayer [39–43].

4.3. Uptake of Be(II) by HCP in the Deg. Stage I: Sorption Isotherms and Effect of S/L Ratio

Sorption isotherms for the uptake of Be(II) by HCP in degradation stage I are shown in Figure 3a for $2 \text{ g}\cdot\text{L}^{-1} \leq S/L \leq 50 \text{ g}\cdot\text{L}^{-1}$. All data represent contact times of $t \geq 60$ days, thus corresponding to equilibrium conditions. In all of the investigated systems, a linear behavior with a slope $\approx +1$ is observed over up to four orders of magnitude in the aqueous Be(II) concentration ($-8 \leq \log [\text{Be(II)}_{\text{aq}}] \leq -4$). In line with the discussion in Section 4.2, this observation supports that Be(II) uptake is controlled by sorption processes and that solubility phenomena do not play any role within the investigated boundary conditions. These results are also consistent with sorption isotherms reported in Çevirim-Papaioannou et al. for HCP in degradation stage II and the C-S-H phases with Ca:Si = 1.0 and 1.6 [33].

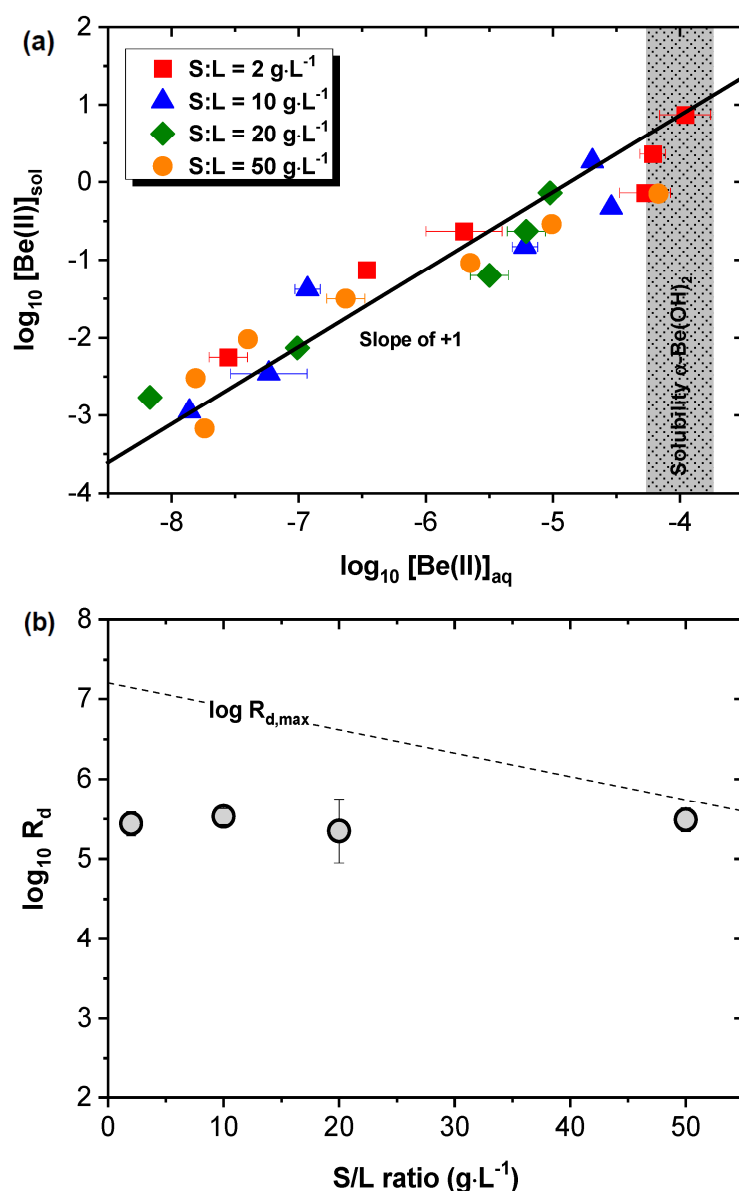


Figure 3. (a) Sorption isotherms of Be(II) taken up by HCP in degradation stage I with $S/L = 2\text{--}50 \text{ g}\cdot\text{L}^{-1}$. Grey regions correspond to the solubility limit of $\alpha\text{-Be(OH)}_2(\text{cr})$ calculated for ACW using thermodynamic data reported in [13]. (b) Values of $\log R_d$ calculated for the uptake of Be(II) by HCP in degradation stage I with $S/L = 2\text{--}50 \text{ g}\cdot\text{L}^{-1}$. Dashed line corresponds to $\log R_{d,\text{max}}$, the highest $\log R_d$ that can be determined at each S:L ratio on the basis of the detection limit of Be(II).

The very high $\log R_d$ values determined in this work ($\log R_d \approx 5\text{--}5.5$, see Figure 3b) are in line with data reported for other strongly sorbing metal ions, mostly M^{3+} and M^{4+} . As initially speculated by Wieland and Van Loon (2003) [18] and extensively discussed in Çevirim-Papaioannou et al. (2021) [33], the similarities in the uptake behavior of Be(II) and apparently very different elements such as Zn(II), Eu(III), Th(IV), or Pu(IV) can be qualitatively explained by the large ratio z/d that they all have ($z/d \geq 1$). For several of these systems, spectroscopic evidence supports the incorporation of the metal ion in the interlayer of the C-S-H structure [39,44,45]. In the case of lanthanides, EXAFS and XRD confirmed the incorporation of Nd(III) into the CaO-layer of C-S-H [46]. This observation is rationalized by the similarities in the ionic radii of Nd^{3+} and Ca^{2+} , i.e., $r_{\text{Nd}^{3+}} = 0.98 \text{ \AA}$ and $r_{\text{Ca}^{2+}} = 1.00 \text{ \AA}$ for CN = 6 [46]. Considering the large differences in the ionic radii of Be^{2+} and Ca^{2+} with CN = 6 ($r_{\text{Be}^{2+}} = 0.45 \text{ \AA}$ and $r_{\text{Ca}^{2+}} = 1.00 \text{ \AA}$), the incorporation of the former in the interlayer of C-S-H is envisaged as the most likely uptake mechanism.

Figure 3b shows similar $\log R_d$ values of Be(II) within the range of the S:L ratios investigated in this work (2–50 $\text{g}\cdot\text{L}^{-1}$). Wieland, Tits, and co-workers observed a decrease in $\log R_d$ for the uptake of Eu(III) and Th(IV) by HCP (deg. stage I) when increasing the S:L ratio from 0.01 to 25 $\text{g}\cdot\text{L}^{-1}$. The authors argued that although the effect seemed experimentally significant, the uncertainty associated with the experimental data prevented them from reaching a final conclusion [17]. In a recently published reference book, Ochs et al. gave credit to the effect described by the PSI team [16] but acknowledged that the mechanism behind this effect is not yet understood. This effect is not observed for Be(II) within the investigated S:L ratios, but its confirmation for other radionuclides or toxic elements could have important implications in repository systems where much higher S:L ratios apply.

4.4. Surface Complexation of Be(II) on C-S-H: Molecular Dynamics Study

The (001) surface is the most energetically stable cleavage plane in C-S-H and thus has an important role in Be(II) uptake by HCP. When Ca:Si is high, the surface is expected to be relatively homogeneous since the silicate layer is composed of dimers with deprotonated silanol groups [47]. Sorption sites for beryllium on the C-S-H (001) surface were identified and described in Çevirim-Papaioannou et al. [33]. It is also important to understand which surface complexes are the most characteristic. Therefore, the running coordination numbers were calculated from the radial distribution functions for individual Be(II) atoms that were close to the surface during the classical molecular dynamics (MD) simulation run. As a distance criterion (the maximum distance), 6 Å from the average position of the deprotonated surface oxygen atoms was chosen. The results are shown in Figure 4. In total, six surface beryllium complexes were identified: three for $\text{Be}(\text{OH})_4^{2-}$ (Be1-Be3) and three for $\text{Be}(\text{OH})_3^-$ (Be4-Be6).

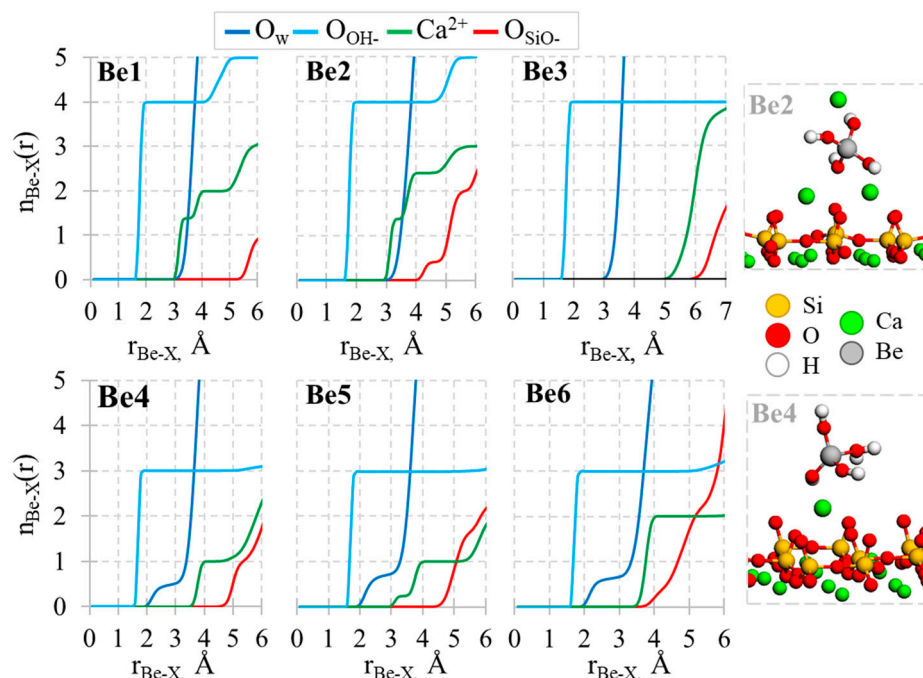


Figure 4. Running coordination numbers for Be-X atom pairs for selected Be atoms. Snapshots of the corresponding Be2 and Be4 surface complexes (water molecules omitted for clarity). O_w and O_{OH^-} correspond to the oxygen atoms in water and hydroxyl-groups, respectively.

The abundance of charge-compensating Ca^{2+} ions creates multiple binding possibilities for anionic species, and the mediation role of Ca^{2+} in the adsorption of highly hydrolyzed metal ions on C-S-H has been already proposed and discussed [33,48]. As it can be seen from Figure 4, all of the observed surface complexes involve at least one

Ca^{2+} cation coordinated with deprotonated silanol groups. For the complexes Be1 and Be2, $\text{Ca}(\text{OH})^+$ was present in the second coordination sphere, increasing the total number of hydroxyl groups to five. On average, $\text{Be}(\text{OH})_4^{2-}$ ions coordinate three Ca^{2+} cations both as inner-sphere (Be1 and Be2) and outer-sphere (Be3) complexes, while $\text{Be}(\text{OH})_3^-$ ions mostly coordinate 1–2 Ca^{2+} . It is apparent that the more surface Ca^{2+} ions that are involved in the complexation, the stronger and closer to the surface Be(II) binding is. The results support our previous experimental and modeling insights well and provide defined target surface species for further free energy of adsorption calculations. These calculations as well as the mechanisms and energetics of beryllium binding on the edge surfaces and in the interlayer of C-S-H will be reported in a separate publication by Androniuk et al. that is presently under preparation.

5. Conclusions

This work represents the first experimental study systematically investigating the uptake of Be(II) by HCP in degradation stage I. This study complements and further extends the previous work by Çevirim-Papaioannou et al. (2021) [33] on the uptake of Be(II) by the C-S-H phases and HCP in degradation stage II.

A very strong sorption of Be(II) (with $\log R_d \approx 5.5$, R_d in $\text{L}\cdot\text{kg}^{-1}$) was observed in all of the investigated systems in spite of the anionic character of the Be(II) hydrolysis species prevailing in the pore water. Very similar observations have been reported for the uptake of Be(II) by C-S-H, unequivocally supporting that this component is the main sink of beryllium in cementitious materials. The results obtained for the uptake of Be(II) by HCP are also in line with data reported for other strongly sorbing elements, e.g., lanthanides, actinides, or other highly charged metal ions. These similarities are qualitatively explained on the basis of the high charge-to-size ratio shared by these metal ions, i.e., $z/d \geq 1$.

Sorption kinetics show a two-step behavior, which can be interpreted by a fast surface complexation process ($t < 4$ days) followed by the slower incorporation of Be(II) in the C-S-H structure ($t \geq 60$ days). A similar uptake sequence has been proposed for other strongly sorbing metal ions such as Zn(II) or An(IV). Additionally, the results of MD simulations confirm that beryllium forms very stable surface complexes on C-S-H and that the number of the coordinated surface Ca^{2+} ions increases the stability and strength of Be(II) binding.

In agreement with our previous study on other cementitious materials [33], the distribution coefficients determined in this work confirm very low Be(II) concentrations in the cement pore water, even in hyperalkaline systems (degradation stage I) characterized by higher beryllium solubility. This experimental study thus fills a relevant knowledge gap affecting the retention/mobilization processes of beryllium in cementitious environments.

Author Contributions: Conceptualization, X.G.; methodology, N.Ç.-P. and I.A.; investigation, N.Ç.-P. and S.H.; writing—original draft preparation, N.Ç.-P. and I.A.; writing—review and editing, N.Ç.-P., I.A., W.U., M.A. and X.G.; supervision, X.G.; project administration, X.G. and M.A.; funding acquisition, M.A. All authors have read and agreed to the published version of the manuscript.

Funding: The research leading to these results received funding from the European Union's European Atomic Energy Community's (Euratom) Horizon 2020 Programme (NFRP-2014/2015) under grant agreement, 662,147–Cebama. The stay of S. Han at KIT–INE was partially funded through the Korea Nuclear International Cooperation Foundation (KONICOF) Nuclear Global Internship Program, the National Research Foundation of Korea funded by the Ministry of Education (NRF-2017M2B2B1072374), and a part of research was supported by the Advanced Nuclear Environment Research Center (ANERC) from the National Research Foundation of Korea (NRF), NRF-2017M2B2B1072374 and NRF-2017M2B2B1072404. We acknowledge support by the KIT-Publication Fund of the Karlsruhe Institute of Technology.

Data Availability Statement: Data is contained within the article.

Acknowledgments: Klas Källström (Swedish Nuclear Fuel and Waste Management Company, SKB) is gratefully acknowledged for providing the cement rod used in this study. Frank Geyer, Annika

Kaufmann, and Cornelia Walschburger (all KIT-INE) are kindly acknowledged for the ICP-MS and ICP-OES measurements.

Conflicts of Interest: The authors declare no conflict of interest.

References

- Walsh, K.A.; Olson, D.L. *Beryllium Chemistry and Processing*; Olson, D.L., Vidal, E.E., Dalder, E., Goldberg, A., Mishra, B., Eds.; ASM International: Novelty, OH, USA, 2009; pp. 20–26.
- Beeston, J.M. Beryllium metal as a neutron moderator and reflector material. *Nucl. Eng. Des.* **1970**, *14*, 445. [[CrossRef](#)]
- Longhurst, G.R.; Carboneau, M.I.; Mullen, C.K.; Sterbentz, J.W. Challenges for disposal of irradiated beryllium. In Proceedings of the 6th IEA Workshop on Beryllium Technology, Mizayaki, Japan, 2–5 December 2003.
- Chandler, D.; Primm, R.T.; Maldonado, G.I. *Reactivity Accountability Attributed to Beryllium Reflector Poisons in the High Flux Isotope Reactor*; ORNL Report TM-2009/188; Oak Ridge Laboratory: Oak Ridge, TN, USA, 2009.
- Gilbert, R.A.; Garrett, A.B. The equilibria of the metastable crystalline form of beryllium hydroxide—Be(OH)₂ in hydrochloric acid, perchloric acid and sodium hydroxide solutions at 25 °C. *J. Am. Chem. Soc.* **1956**, *78*, 5501–5505. [[CrossRef](#)]
- Kakihana, H.; Sillen, L.G. Studies on the Hydrolysis of Metal Ions. 16. The Hydrolysis of the Beryllium Ion, Be²⁺. *Acta Chem. Scand.* **1956**, *10*, 985–1005. [[CrossRef](#)]
- Schwarzenbach, G.; Wenger, H. Die protonierung von metall-aquaionen I.: Be·aq²⁺ solvatations-isomerie. *Helv. Chim. Acta* **1969**, *52*, 644. [[CrossRef](#)]
- Bruno, J. Beryllium(II) hydrolysis in 3.0 mol·dm⁻³ perchlorate. *J. Chem. Soc. Dalton Trans.* **1987**, *10*, 2431–2437. [[CrossRef](#)]
- Bruno, J.; Grenthe, I.; Sandstrom, M.; Ferri, D. Studies of Metal Carbonate Equilibria. 15. The Beryllium(II)—Water-Carbon Dioxide(g) System in Acidic 3.0 mol dm⁻³ Perchlorate Media. *J. Chem. Soc. Dalton Trans.* **1987**, *10*, 2439–2444. [[CrossRef](#)]
- China, E.; Dominguez, S.; Mederos, A.; Brito, F.; Sanchez, A.; Ienco, A.; Vacca, A. Hydrolysis of beryllium(II) in DMSO:H₂O. *Main Group Met. Chem.* **1997**, *20*, 11–17. [[CrossRef](#)]
- Bruno, J.; Grenthe, I.; Munoz, M. Studies of Metal Carbonate Equilibria. Part 16. The Beryllium(II)—Water-Carbon Dioxide(g) System in Neutral-to-Alkaline 3.0 mol dm⁻³ Perchlorate Media at 25 °C. *J. Chem. Soc. Dalton Trans.* **1987**, *10*, 2445–2449. [[CrossRef](#)]
- Green, R.W.; Alexander, P.W. Hydrolysis of Bis-(Acetylacetonato)-Beryllium(II). *J. Phys. Chem.* **1963**, *67*, 905. [[CrossRef](#)]
- Cevirim-Papaioannou, N.; Gaona, X.; Böttle, M.; Yalcintas Bethune, E.; Schild, D.; Adam, C.; Sittel, T.; Altmaier, M. Thermodynamic description of Be(II) solubility and hydrolysis in acidic to hyperalkaline NaCl and KCl solutions. *Appl. Geochem.* **2020**, *117*, 1–13. [[CrossRef](#)]
- Atkinson, A.; Everitt, N.; Guppy, R. *Evolution of pH in a Rad-Waste Repository: Internal Reactions between Concrete Constituents*; UKAEA Report AERE-R12939; AEA Technology: Harwell, UK, 1988; pp. 100–113.
- Berner, U.R. Evolution of porewater chemistry during degradation of cement in a radioactive waste repository environment. *Waste Manag.* **1992**, *12*, 201–219. [[CrossRef](#)]
- Ochs, M.; Dirk, M.; Wang, L. *Radionuclide and Metal Sorption on Cement and Concrete*; Springer: Switzerland, 2016.
- Tits, J.; Wieland, E. *Actinide Sorption by Cementitious Materials*; PSI Technical Report 18-02; Paul Scherrer Institute: Villigen, Switzerland, 2018.
- Wieland, E.; Van Loon, L. *Cementitious Near-Field Sorption Data Base for Performance Assessment of an ILW Repository in Opalinus Clay*; Technical Report 03-06; Paul Scherrer Institut: Villigen, Switzerland, 2003.
- Wieland, E. *Sorption Data Base for the Cementitious Near Field of L/ILW and ILW Repositories for Provisional Safety Analyses for SGT-E2*; Nagra Technical Report 14-08; Paul Scherrer Institut: Villigen, Switzerland, 2014.
- Bues, M.; Doubre, H.; Panet, M.; Poty, B. *Dossier 2005 Argile Tome: Évaluation de Sécurité du Stockage Géologique*; Andra: Châtenay-Malabry, France, 2005.
- Ahlford, K.; Herschend, B.; Källstöm, K.; Mårtensson, P.; von Schenck, H. *Initial State for the Repository for the Safety Evaluation SE-SFL*; SKB Technical Report (TR-19-03); SKB: Solna, Sweden, 2019.
- Brandefelt, J.; Ekström, P.-A.; Hedström, S.; Hjerne, O.; Lindgren, H.; Saetre, P.; Shahkarami, P.; Wessely, O. *Radionuclide Transport and Dose Calculations for the Safety Evaluation SE-SFL*; SKB Technical Report (TR-19-06); SKB: Solna, Sweden, 2019.
- Brandefelt, J.; Hedström, S.; Lindgren, G.; Marsic, N. *Post-Closure Safety for a Proposed Repository Concept for SFL. Main Report for the Safety Evaluation*; SKB Technical Report (TR-19-01); SKB: Solna, Sweden, 2019.
- Petterson, M.; Skagius, K.; Moreno, L. *Analysis of Radionuclide Migration from SFL 3-5*; SKB Report (R-99-14); SKB: Stockholm, Sweden, 1999.
- Skagius, K.; Petterson, M.; Wiborgh, L.; Albinsson, Y.; Holgersson, S. *Compilation of Data for the Analysis of Radionuclide Migration from SFL 3-5*; SKB Report (R-99-13); SKB: Stockholm, Sweden, 1999.
- Shannon, R.D. Revised Effective Ionic Radii and Systematic Studies of Interatomic Distances in Halides and Chalcogenides. *Acta Cryst.* **1976**, *A32*, 751–767. [[CrossRef](#)]
- Hunter, F.M.; Jackson, P.C.; Kelly, M.; Williams, S.J. *A Post-Closure Toxicity Screening Assessment for the Nirex Phased Geological Disposal Concept*; Serco Assurance Report for Nirex (SA/ENV-0854 for NDA RWMD); NDA: Harwell, UK, 2006.
- Generic Repository Studies: Generic Post-Closure Performance Assessment*; Nirex Report N/080; Nirex: Harwell, UK, 2003.
- Tasi, A.; Gaona, X.; Rabung, T.; Fellhauer, D.; Rothe, J.; Dardenne, K.; Lützenkirchen, J.; Grivé, M.; Colàs, E.; Bruno, J.; et al. Plutonium retention in the isosaccharinate-cement system. *Appl. Geochem.* **2021**, *126*, 1–17. [[CrossRef](#)]

30. Lagerblad, B.; Trägårdh, J. *Conceptual Model for Concrete Long Time Degradation in a Deep Nuclear Waste Repository*; SKB Technical Report (TR-95-21); SKB: Stockholm, Sweden, 1994.
31. *Safety Analysis for SFR Long-Term Safety*; SKB Technical Report (TR-14-01); SKB: Stockholm, Sweden, 2015.
32. Jamil, T.; Javadi, A.; Heinz, H. Mechanism of molecular interaction of acrylate-polyethylene glycol acrylate copolymers with calcium silicate hydrate surfaces. *Green Chem.* **2020**, *22*, 1577–1593. [[CrossRef](#)]
33. Cevirim-Papaioannou, N.; Androniuk, I.; Han, S.; Ait Mouheb, N.; Böttle, M.; Gaboreau, S.; Claret, F.; Gaona, X.; Böttle, M.; Altmaier, M. Surface Processes Driving the Uptake of Beryllium by Cement, C-S-H Phases and TiO₂: Wet-Chemistry and Molecular Dynamics Studies. *Chemosphere* **2021**, *282*, 131094. [[CrossRef](#)]
34. Cygan, R.T.; Liang, J.J.; Kalinichev, A.G. Molecular models of hydroxide, oxyhydroxide, and clay phases and the development of a general force field. *J. Phys. Chem. B* **2004**, *108*, 1255–1266. [[CrossRef](#)]
35. Kalinichev, A.G.; Wang, J.W.; Kirkpatrick, R.J. Molecular dynamics modeling of the structure, dynamics and energetics of mineral-water interfaces: Application to cement materials. *Cem. Concr. Res.* **2007**, *37*, 337–347. [[CrossRef](#)]
36. Mishra, R.K.; Mohamed, A.K.; Geissbuhler, D.; Manzano, H.; Jamil, T.; Shahsavari, R.; Kalinichev, A.G.; Galmarini, S.; Tao, L.; Heinz, H.; et al. A force field database for cementitious materials including validations, applications and opportunities. *Cem. Concr. Res.* **2017**, *102*, 68–89. [[CrossRef](#)]
37. Plimpton, S.; Hendrickson, B.; Bolding, B. A New Parallel Molecular-Dynamics Algorithm for Simulation of Organic Materials. *Abstr. Pap. Am. Chem. Soc.* **1994**, *208*, 4-Comp.
38. Giffaut, E.; Grive, M.; Blanc, P.; Vieillard, P.; Colas, E.; Gailhanou, H.; Gaboreau, S.; Marty, N.; Made, B.; Duro, L. Andra thermodynamic database for performance assessment: ThermoChimie. *Appl. Geochem.* **2014**, *49*, 225–236. [[CrossRef](#)]
39. Gaona, X.; Dahn, R.; Tits, J.; Scheinost, A.C.; Wieland, E. Uptake of Np(IV) by C-S-H Phases and Cement Paste: An EXAFS Study. *Environ. Sci. Technol.* **2011**, *45*, 8765–8771. [[CrossRef](#)]
40. Pointeau, I.; Landesman, C.; Giffaut, E.; Reiller, P.; Coreau, N.; Moisan, C.; Reiller, P. *Etude de la Retention Chimique des Radionucléides Cs(I), Am(III), Zr(IV), Pu(IV), Nb(V), U(VI) et Tc(IV) par es Matériaux Cimentaires Dégradés*; Rapport Technique RT DPC/SECR 03-037; CEA: Saclay, France, 2004.
41. Schlegel, M.L.; Pointeau, I.; Coreau, N.; Reiller, P. Mechanism of europium retention by calcium silicate hydrates: An EXAFS study. *Environ. Sci. Technol.* **2004**, *38*, 4423–4431. [[CrossRef](#)]
42. Tits, J.; Geipel, G.; Mace, N.; Eilzer, M.; Wieland, E. Determination of uranium(VI) sorbed species in calcium silicate hydrate phases: A laser-induced luminescence spectroscopy and batch sorption study. *J. Colloid Interface Sci.* **2011**, *359*, 248–256. [[CrossRef](#)]
43. Ziegler, F.; Giere, R.; Johnson, C.A. Sorption mechanisms of zinc to calcium silicate hydrate: Sorption and microscopic investigations. *Environ. Sci. Technol.* **2001**, *35*, 4556–4561. [[CrossRef](#)]
44. Tits, J.; Stumpf, T.; Rabung, T.; Wieland, E.; Fanghanel, T. Uptake of Cm(III) and Eu(III) by calcium silicate hydrates: A solution chemistry and time-resolved laser fluorescence spectroscopy study. *Environ. Sci. Technol.* **2003**, *37*, 3568–3573. [[CrossRef](#)]
45. Ziegler, F.; Scheidegger, A.M.; Johnson, C.A.; Dahn, R.; Wieland, E. Sorption mechanisms of zinc to calcium silicate hydrate: X-ray absorption fine structure (XAFS) investigation. *Environ. Sci. Technol.* **2001**, *35*, 1550–1555. [[CrossRef](#)]
46. Mandaliev, P.; Wieland, E.; Dahn, R.; Tits, J.; Churakov, S.V.; Zaharko, O. Mechanisms of Nd(III) uptake by 11 angstrom tobermorite and xonotlite. *Appl. Geochem.* **2010**, *25*, 763–777. [[CrossRef](#)]
47. Grangeon, S.; Fernandez-Martinez, A.; Baronnet, A.; Marty, N.; Poulain, A.; Elkaim, E.; Roosz, D.; Gaboreau, S.; Henocq, P.; Claret, F. Quantitative X-ray pair distribution function analysis of nanocrystalline calcium silicate hydrates: A contribution to the understanding of cement chemistry. *J. Appl. Crystallogr.* **2017**, *50*, 14–21. [[CrossRef](#)]
48. Androniuk, I.; Kalinichev, A.G. Molecular dynamics simulation of the interaction of uranium (VI) with the C-S-H phase of cement in the presence of gluconate. *Appl. Geochem.* **2020**, *113*, 104496. [[CrossRef](#)]